

BRIDGING BETWEEN MICRO- AND MACROSCALES OF MATERIALS BY MESOSCOPIC MODELS

B. I. Lundqvist^{*1}, A. Bogicevic[§], S. Dudiy^{*}, P. Hyldgaard^{*}, S. Ovesson^{*}, C. Ruberto^{*}, E. Schröder^{*}, and G. Wahnström^{*}

^{*}Department of Applied Physics, Chalmers University of Technology and Göteborg University, S-412 96 Göteborg, Sweden

[§]Scientific Research Laboratory, Ford Motor Company, Dearborn, MI 48121-2053, USA

Abstract

The importance of bridging length scales for materials is illustrated by three examples, nematic liquid crystals, strength of materials, and epitaxial growth. Emphasis is on the microscopic scale, with first-principles calculations of molecule-surface interaction, stacking-fault energies, interlayer interactions, diffusion barriers, and adsorbate-adsorbate interactions. Some pilot examples of using such information on the meso- and macroscales with models using director fields, misfit densities of dislocation, and monomer and island densities are presented. The area is predicted to have a great future.

Keywords: Materials, length scales, liquid crystal, strength of materials, growth.

¹Corresponding author: Tel. +46 31 772 3188; Fax: +46 31 772 8426; E-mail: lundqvist@fy.chalmers.se

1. Introduction

Materials theory, modelling, and simulations is an area in rapid development: In that process multiscale modelling is a necessity. The gaps between micro-, meso-, and macroscopic scales have to be bridged, in order to fully implement the immense potential of computational materials theory. This is not only an inherent option and obligation of the field. Technologically, materials behavior thus modelled might imply reduced costs for fabrication and increased manufacturing efficiencies.

One way to multiscale modelling is computational design of hierarchically structured materials [1], a systems approach that integrates processing, structure, property, and performance relations. For, *e.g.*, high-performance alloy steels, numerical implementation of materials-science principles provides a hierarchy of computational models that define subsystem design parameters that are integrated, through computational thermodynamics, in the comprehensive design of materials as interactive systems. Another approach uses mesoscale simulation to predict microstructure and microstructure evolution during thermodynamical processes. Such an approach can be based on coupling parts by a finite-element-method (FEM) deformation model at the microstructural length scale with a Monte-Carlo simulation of the evolution of the deformation substructure during annealing.

This paper advocates the use of multiscale modelling and simulation based on (i) general macroscopic descriptions, such as those for elasticity, electromagnetism, hydrodynamics, and rheology, (ii) insightful modifications of the applicable field theory on the mesoscopic scale, and (iii) microscopic theory to provide key parameters emanating from atomic-scale behavior.

As we are engaged in microscopic descriptions of nature, bridging for us primarily means the latter type of approach, starting with first-principles calculations. Our materials consortium's scope to bridge the scales has so far only been filled with some pilot studies. As an indication

of what can be done, three examples produced in our group are briefly reviewed, concerning (i) liquid crystals, (ii) strength of materials, and (iii) crystal growth. In these cases the micro-, meso-, and macroscales can be illustrated by molecule-surface interaction, director field, and optical properties in displays, stacking fault, misfit density of dislocation, and strength, and diffusion barriers, island density, and crystal growth, respectively.

2. Director configuration of nematic liquid crystal

The nematic liquid crystal (NLC) state of matter is the simplest state with an anisotropic electromagnetic response. In NLC elongated molecules have random positions but align themselves along an average direction, giving the NLC directional order and positional isotropy, manifested in, *e.g.*, various biological molecules and membranes, surfactants, and emulsifiers, and in extensive technological applications in, *e.g.*, optical displays. It is important to provide a mesoscopic NLC link between micro- and macroscopic descriptions in a simple model.

An analytical NLC link, describing the NLC configuration as a function of anchoring conditions, has been derived for the NLC confined between two planar plates [2]. Ultimately, a first-principles account of the molecule-surface interaction is strived for, but the present account gives the behavior as a function of the material constants and the molecular directions at the boundaries (anchoring angles). The general analytical solution is derived in terms of Legendre third elliptic functions of the variation in average molecular direction within the NLC (Fig. 1).

The analytical solution for the molecular directions has several important implications: (i) as it is given in established special functions, it is easily available; (ii) the NLC system can be efficiently and extensively analyzed; and (iii) the dependence of the system behavior on materials and system parameters can be obtained, exemplified by results for the dependence of the optical transmission on parameters like the strength of the applied field, the elastic coefficients, and the anchoring angles (Fig. 2).

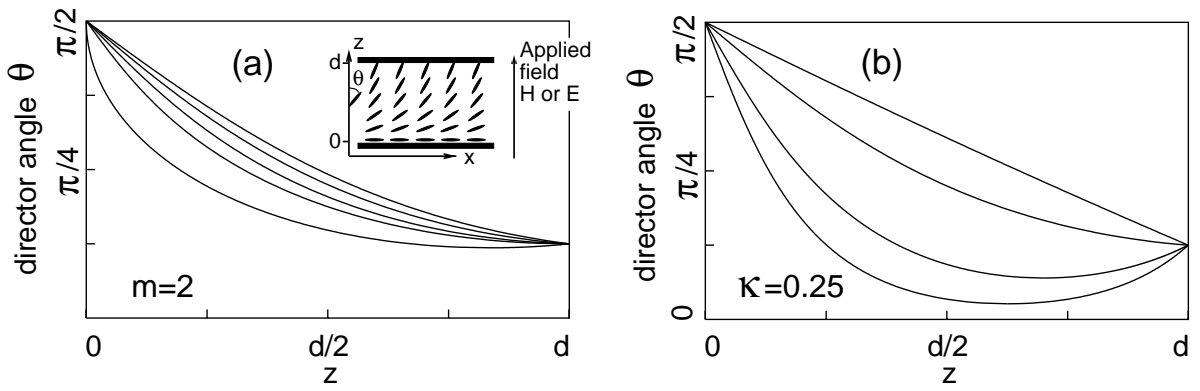


Figure 1: The NLC director field. (a) The director angle θ versus the vertical position z . At fixed reduced magnetic potential $m = (\mu_a \mu_0 / K_3)^{1/2} H d = 2$ or reduced voltage $m = (\varepsilon_a \varepsilon_0 / K_3)^{1/2} E d = 2$ the value of the elastic anisotropy runs through $\kappa = (K_3 - K_1) / K_3 = 0, 0.25, 0.5, 0.75, 1$ (top to bottom curves) where K_1 is the splay elastic constant and K_3 the bend elastic constant. The insert illustrates the system of parallel plates encompassing the NLC, in this case with top anchoring at $\pi/8$ and bottom anchoring at $\pi/2$. The director field is represented by small sticks. (b) The director angle $\theta(z)$ at fixed elastic anisotropy $\kappa = 0.25$ for applied fields $m = 0$ (top curve), 2, 4, and 6 (bottom curve).

Macroscopically, the NLC may be described by a continuous vector field $\mathbf{n}(\mathbf{r})$, a director field, representing the local average direction of the molecules at position \mathbf{r} . For symmetry reasons, $\mathbf{n}(z) = (\sin \theta(z), 0, \cos \theta(z))$, where θ is the angle between the director and the z -axis (Fig. 1). From the Helmholtz free energy and the Euler-Lagrange equations a relation between the angle θ and the z -position is then obtained. The bulk splay and bend elastic coefficients of the NLC are accounted for.

The analytical expression for the director angle of a NLC confined between parallel plates, with general nontwist anchoring conditions, provides an explicit link between atomic-scale properties at the plate interface to macroscopic bulk behavior, thereby bridging the gap between micro- and macroscales.

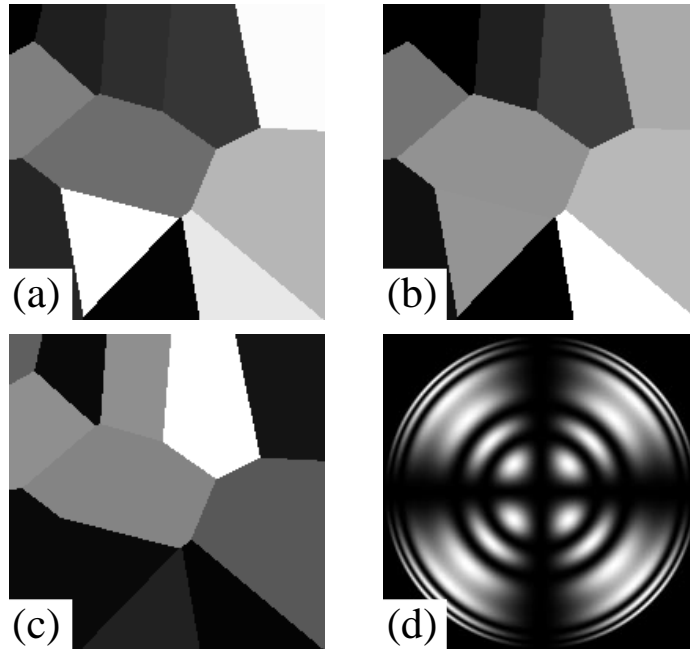


Figure 2: Theoretical predictions of the intensity of polarized light transmitted through (a) a thin NLC film on top of an inhomogeneous substrate or (d) a wetting droplet. (a) No applied field. (b) External field applied perpendicular to the film. (c) Polarization turned 45° with respect to (a). (d) Droplet on a self-assembled monolayer (SAM) of organic molecules. The intensity profile agrees very well with experiments and simulations.

3. Strength of materials

Mechanical properties of materials depend hierarchically on phenomena with length scales from atomic up to macroscopic ones. Extended defects, such as dislocations and grain boundaries, are key actors for large-scale behavior of solids, like plasticity, fracture, and the brittle-ductile transition. Theory is challenged to connect experimentally observed macroscopic properties to microscopic ones of extended defects, whose atomic-scale properties today successively get accessible for studies with electron-structure theory. At large distances continuum elasticity theory describes dislocation properties and dislocation interactions in a useful way. At the other extreme, an atomistic description is required for the material specific, discrete atomic-core structure of the dislocation. Peierls proposed early a hybrid model, [3] where some details of the discrete dislocation core are incorporated in an essentially continuum framework. The analytic solution of this Peierls-Nabarro (PN) model [4] gives a meaningful estimate of the lattice resistance to dislocation motion.

3.1 Dislocations

Dislocations are key concepts for the understanding of mechanical properties of crystalline solids. The PN model [3, 4] provides a conceptual framework for dislocation structure and energetics. It is essentially a continuum treatment, but the dislocation core, the region of inelastic displacement, is given an approximate atomistic description. The forces in the core, where the atomic-scale discreteness really counts, are currently approximated with the generalized stacking-fault (GSF) surface [5, 6], which is the interplanar potential-energy for sliding one half of a crystal over the other half.

Mechanical properties are not only affected by dislocations. Grain-boundary sliding is another possible mechanism. Also here analogous mesoscopic descriptions exist.

The bridging is here first exemplified for elementary semiconductors and metals. In fcc metals

the experimentally observed dislocations have planar cores and should therefore be favorable cases for the PN model. However, in practice mechanical strength of close-packed metals is not determined by the intrinsic resistance to dislocation motion but depends on extrinsic obstacles, such as solute atoms, grain boundaries, and precipitates, which block the motion of the dislocations. In stronger covalent, ionic, and intermetallic crystals the plastic properties directly depend on nucleation and mobility of dislocations. The intrinsic mobility is also an important factor for creep behavior. All these additions of course affect the PN description.

Generalizations of the PN model and first-principles calculations on precipitates and interfaces are also touched upon.

3.2 Dislocation in Si

The nature of dislocations in silicon is an object for frequent studies. In Ref. [7] the interaction between two partial 90° edge dislocations is studied with atomic-scale simulations using the effective-medium tight-binding method. A large separation between the two dislocations (up to 30 Å, comparable to experimental values) is achieved with a solution of the tight-binding Hamiltonian that scales linearly with the number of atoms. The partial edge dislocation is found to be very accurately described by the PN dislocation model, using the calculated GSF restoring forces, as reflected both in the interaction energy and in the displacement field. An asymmetric core reconstruction provides fourfold coordination, making Si behave elastically down to atomic distances [7].

3.3 Dislocations in metals

The GSF surface plays an important role in proposed models for the brittle-ductile transition, and they can also be used for calibration of model potentials for large-scale simulations and as input to quasicontinuum models [8].

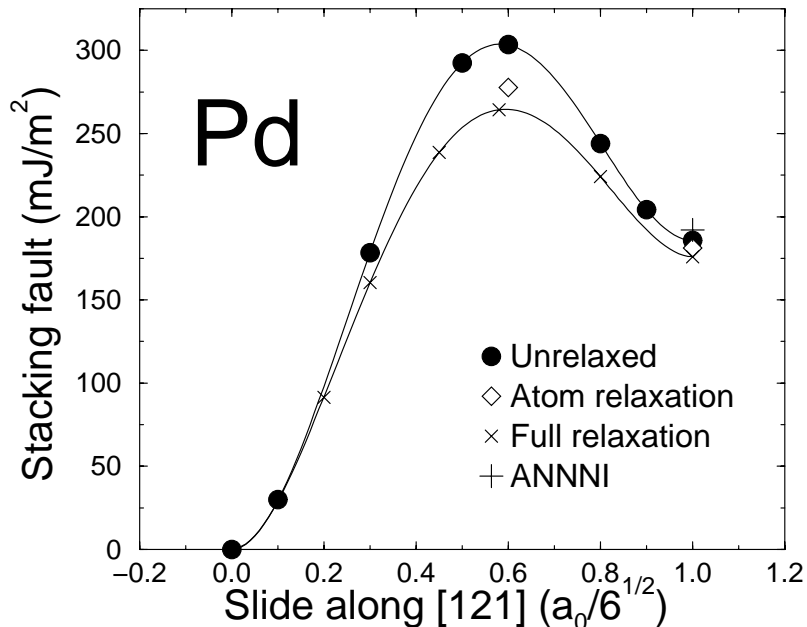


Figure 3: Generalized-stacking-fault (GSF) curve for Pd sliding in the [121] direction on the (111) plane [8], calculated for unrelaxed lattice and for various degrees of relaxations described in Ref. [8], where also the Ising-model-type calculation (ANNNI) is described.

Accurate input to the PN model can be provided by the density-functional theory (DFT). In this theory the complex many-electron problem is replaced by a simpler one, where a functional of the electron density is minimized. Methodological advancement of DFT together with the improved performance of computers and numerical methods make it realistic to address the present types of questions from first principles.

The DFT has been used to calculate GSF curves for both unrelaxed and relaxed Pd and Al along main crystal directions ([121] and [110]) [8], including dislocation profiles (Fig. 3), and barriers and stresses for dislocation motion. The GSF curves are applied in the PN model to Shockley partials and edge dislocations. The results for Peierls stresses compare well with experimental values. Two dissociated partial dislocations are shown to be strongly elastically coupled in their motion. These interactions have effects on the Peierls barrier [8].

3.4 Peierls-Nabarro model and generalizations

The PN model provides a conceptual framework, and with atomic forces derived from the GSF surface, dislocation properties can be determined quantitatively. For planar dislocations the PN model gives a continuum solution for the dislocation $f_b(x)$, from which a misfit energy can be computed and thus also energy barriers and stresses for dislocation motion. A dislocation introduced into a lattice generates stresses at the interface/glide plane, which are calculated according to elasticity theory. These elastic stresses are balanced by atomic forces acting on either side of the glide plane due to the misfit of atomic planes. This is expressed in an integrodifferential equation for the misfit density per unit area, or dislocation profile, $\rho_b(x) = df_b(x)/dx$, [3, 4, 9]

$$\frac{K_b}{2\pi} \int_{-\infty}^{\infty} \rho_b(x') \frac{1}{x-x'} dx' = F_b(f_b(x)). \quad (1)$$

The constant K_b determines the magnitude of the elastic stresses caused by introducing the dislocation and is possible to determine by solving the elastic equations for the anisotropic case [9, 10]. The dislocation is viewed as a distribution of infinitesimal Burgers vectors $\rho_b(x)dx$, with the misfit density normalized as $\int_{-\infty}^{\infty} \rho_b(x)dx = b$, the length of the appropriate Burgers vector. The restoring atomic forces on the right-hand side of Eq. (1) may be approximated by the appropriate GSF curve, [5, 6] from

$$F_b(f_b(x)) = -\frac{\partial \gamma_{GSF}(f_b(x))}{\partial f_b}, \quad (2)$$

where γ_{GSF} is obtained by calculating the energy change, when the system is sliding on the glide plane in the direction of the Burgers vector.

A study of Shockley partials in Pd with both a full-scale atomistic simulation of the structure and energetics of the dislocation motion and the PN model shows the two approaches to result in substantial differences [11]. In this case a reasonable improvement of the PN model is to solve the ordinary PN equation, but with atomic forces evaluated for a disregistry that corresponds to extrapolated positions of the atomic planes according to Eq. (1) but with a disregistry

$f_b(x; y)$ calculated for atoms located at a finite distance $y = \pm d/2$, above and below the glide plane, respectively [11]. Thus extrapolation of the results from the PN model to the real atomic positions using elasticity theory gives a better agreement [11]. A consistency could be obtained by modifying the original PN model and using the extrapolated disregistry positions in the expression for the restoring atomic forces. This modification improves the core structure considerably and would probably have quantitative capabilities [11].

When critically examined, the classical Peierls-Nabarro theory of dislocations has a number of inconsistencies [12]. A semidiscrete theory corrects the inconsistencies of the classic theory and gives results similar to actual atomistic calculations, both qualitatively and quantitatively, and provides a link between accurate nanometer-scale quantum mechanical calculations of the dislocation core energetics to mesoscale continuum descriptions [12]. It would be interesting to combine the semidiscrete PN model and the above modification for the simple-fcc-metal case to validate the PN model. A well-working PN model would be able to give trends for dislocation properties with input from first-principles GSF surfaces and could be a useful tool for 'screening'/correlating mechanical properties from a reliable atomistic input.

3.5 Strength of real materials

In the bridging interfaces are key mesoscale features. Knowledge of interface structure and energetics is important for modelling of both nucleation and growth in complex alloys and of their strength and other mechanical properties, such as high-temperature creep resistance.

Precipitates: In steels, non-shearable precipitates are obtained with carbide and nitride formers, such as Ti, V, Cr, and Nb. Precipitates with the nacl structure is one important class and are often found as small thin discs (radius $\simeq 50\text{-}100 \text{ \AA}$). The 'flat' part of the interface is semi-coherent (that is, has a small misfit-dislocation density), whereas the 'side' of the disc has a large lattice mismatch and is incoherent with the Fe matrix.

The electronic and atomic structures of a model system consisting of the semi-coherent interface between bcc-Fe and nacl-VN have been calculated with a pseudopotential implementation of DFT [13]. A key result is the very small, and even negative, value of the interface energy [13]. This does not only find its natural interpretation in electron-structural terms but is also consistent with experimental observations. In this way one points out key features of the electron structure that make the formation of VN precipitates in Fe favorable, which in turn is important to make steel tough.

This kind of modelling may thus be used to predict long-time structural changes in steels in order to improve high-temperature creep resistance. The thermodynamical modelling should also include elastic energies due to volume differences, which is often done separately. In contrast, a real interface has more degrees of freedom and may, for instance, create misfit dislocations.

Interfaces: Highly relevant in industry, the problem of metal-ceramic adhesion has attracted considerable materials-science attention, in particular to rationalize the adhesion strength in terms of the interface atomic and electronic structures. While, *e.g.*, most oxides are isolating ionic crystals, the transition-metal carbides are characterized by covalent bonding mixed with metallicity and slight ionicity, which makes the mechanism of the metal-carbide adhesion very particular. Sintered hard metals, an extraordinarily successful powder-technological product, are produced by compressing pellets of metals, like Co, and metal carbides, *e.g.*, WC and TiC.

Recently, one such class, the interface between a transition metal and a transition-metal carbide, has been addressed in an *ab initio* theoretical study of the representative Co/TiC(001) interface [14, 15, 16, 17]. These first-principles computational experiments are based on DFT with GGA-PW91 and consist of several steps: (i) performing total-energy calculations on a large number of hypothetical but realistic structures of the Co/TiC interface, (ii) allowing the atoms to relax under the given, available external conditions, (iii) analyzing the structural,

bonding, and energetic results with respect to trends and idealized electron-structure models, and (iv) deducing general results akin to the available experimental experiences. They allow the origin of the adhesion strength to be traced down from the specifics of the interface atomic and electronic structure. Especially interesting findings concern the interface Co-C bonds, which are unexpectedly strong and play a crucial role in the energetics and the atomic structure of the Co/TiC(001) interface. At the same time the strength of the Co-C bonds comes from intrinsic interfacial effects that can be clearly identified in the electronic structure. The effective number of these bonds is controlled by an interplay between lattice mismatch and the relaxation effects. The calculated adhesion strength agrees reasonably well with results of wetting experiments.

Detailed analyses of local densities of states (LDOS) show that there is a new interfacial effect at work: The interface Co-C bonds are much stronger than the bulk ones. In bulk CoC the Co-C antibonding states are derived mainly from the Co-*d* states. The interface Co-C bonds have a large concentration of the delocalized metallic states of Co in the region of space and energy, where the Co-C antibonding states could be located. Thus the localization of the Co-C antibonding states inside a small space-energy region is unfavorable due to the Pauli principle. Thus the interface Co-C antibonding states should be much more delocalized than the bulk ones, losing their antibonding character.

First-principles interface calculations like these should be possible to extend to the calculation of atomic-scale parameters for mechanical properties.

4. Crystal growth

Nucleation and growth of epitaxial films are of great practical and fundamental interest. In systems, where the overlayer wets the substrate, *i.e.* in layer-by-layer or Frank-van der Merwe growth, the islands are only one atomic layer thick, with morphologies ranging from ramified structures at low temperatures to compact, polygonal shapes at higher temperatures. The great

variety reflects the complex nature of the dynamical processes in such non-equilibrium systems. Experimental techniques, like scanning-tunnelling microscopy (STM), low-energy-electron microscopy, low-energy-electron diffraction (LEED), and grazing-incidence x-ray scattering, allow studies of evolving adlayers for length scales ranging from angstroms to microns, and times ranging from picoseconds to minutes. This provides opportunities for developing quantitative theories for thin-film growth, which ideally should span these length and time scales to connect first-principles electron-structure calculations with thin-film morphology. This is attempted by with first-principles calculations, kinetic Monte-Carlo simulations, rate equations, and scaling theory.

Models of epitaxial growth under typical molecular-beam-epitaxy (MBE) conditions commonly assume that atoms are deposited randomly onto an initially flat substrate at a constant rate of F monolayers/sec and diffuse freely on the crystalline substrate, until they encounter another atom, a group of atoms or a defect, like a step. The population of isolated adatoms increases initially linearly with time, until small islands begin to nucleate. During the "aggregation time", *i.e.* the time span when the number of islands increases due to increasing deposition but with this number still smaller than the number of monomers, the film growth can be characterized by the dynamical evolution of the island-size distribution, island shapes, and locations.

Our examples here primarily concern attempts to understand the effects of elementary atomic-scale processes on the island shapes and distributions, since these islands form the building blocks upon which all further growth proceeds. As the morphology of the first monolayer has a great influence on the nucleation and growth of the second and subsequent layers, we also give an example of interlayer couplings.

4.1 Mesoscale descriptions

The island size distribution function $\langle n_s(\theta) \rangle$, where the brackets represent an average over a

large area of the surface or an ensemble of systems, is defined as the number of islands per unit area containing s atoms at a coverage $\theta = Ft$. One way to describe its dynamical evolution is by a set of deterministic coupled rate equations. The rate coefficients that are inputs into these equations should contain information about all of the atomic-scale processes, as well as long-range correlations between islands. The problem is a complex one and approximations have to be made. The rate equations describe the time evolution during early times up until the islands start to coalesce, typically replacing time by coverage $\theta = Ft$. Equations for the coverage derivative of $\langle n_s(\theta) \rangle$ can be set up in terms of the adatom-diffusion constant D , flux F , and the capture numbers σ_s , expressing the efficiency of an island of size s in competing for the available monomers on the surface. They contain terms for the rate at which diffusing monomers are added to an island of size $s - 1$ (s) multiplied by the total density of islands of that size, processes that increase (decrease) the number of islands of size s , and terms that account for the direct capture of deposited atoms by islands of size $s - 1$ and s , respectively.

In particular, the equation for the density of monomers can be written [18]

$$\frac{d\langle n_1 \rangle}{d\theta} = 1 - 2\left(\frac{D}{F}\right)\sigma_1\langle n_1 \rangle^2 - \left(\frac{D}{F}\right)\langle n_1 \rangle \sum_{s=2}^{\infty} \sigma_s \langle n_s \rangle - \kappa_1 \langle n_1 \rangle - \sum_{s=1}^{\infty} \kappa_s \langle n_s \rangle, \quad (3)$$

where the terms on the right-hand side account for the flux of atoms onto the surface, for the loss of monomers to dimer formation, for that to attachment to islands, for the loss of diffusing monomers due to direct capture of the deposited flux, and for the loss of flux to the direct impingement onto existing islands and monomers, respectively. The factor of 2 in the second term describes the fact that when one dimer is formed two monomers are lost.

Any information about island structure and spatial correlation between islands has to be contained in the time-dependent capture numbers σ_s . As the average quantities $\langle n_s(\theta) \rangle$ contain incomplete information about the correlations, the system of equations (3) has to be augmented with further information or assumptions, as is done in numerous approximations in the literature. Typically, a mean-field assumption is made, for instance, as in the following model [18]:

Consider a circular island of radius R_s that is embedded in an ensemble-averaged system of islands and monomers. The local density of monomers, $n_1(\mathbf{r}, \theta)$, responds to the presence of this island. In particular, if adatoms attach irreversibly, the density of monomers vanishes at the edge of the island, $n_1(R_s, \theta) = 0$. The simplest possible diffusion equation describing the spatial variations of n_1 is

$$\frac{\partial n_1}{\partial \theta} = \left(\frac{D}{F}\right) \nabla^2 n_1 + j - \left(\frac{D}{F}\right) \xi^{-2} n_1, \quad (4)$$

where j and ξ can be calculated from the self-consistency condition, $n_1(r \rightarrow \infty, \theta) = n_1(\theta)$, *i.e.* the presence of this island is not felt infinitely far away. In this limit, Eq. (4) must reproduce Eq. (3), which leads to

$$j = 1 - \sum_{s=1}^{\infty} \kappa_s \langle n_s \rangle \quad (5)$$

and

$$\xi^{-2} = 2\sigma_1 \langle n_1 \rangle + \sum_{s=2}^{\infty} \sigma_s \langle n_s \rangle + \left(\frac{D}{F}\right) \kappa_1, \quad (6)$$

where ξ is the average distance a monomer travels before being captured by an island or another monomer and j is the fraction of the flux, which lands on the bare substrate. In this approach the mean-field assumption that at every point outside the island, the local densities $n_s(\mathbf{r}, \theta)$ taking on their average values $\langle n_s(\theta) \rangle$ (for $s \geq 2$) is implicit.

Despite "simplicity", Eq. (4) is difficult to solve, due to its complicated time dependence [$\xi = \xi(t)$] and the growth of the island, *i.e.* the moving boundary. An approximate solution can be found, however, by assuming that the rate of adatom diffusion is large compared to the growth rate of the island. It is sufficient then to fix the radius of the island and solve for the instantaneous concentration of monomers. One cannot satisfy Eq. (4), as $r \rightarrow \infty$, if the coverage (time) derivative of the more general $n(r, \theta)$ is neglected. Instead, subtracting Eq. (3) from Eq. (4),

$$\frac{F}{D} \left(\frac{\partial n_1}{\partial \theta} - \frac{d\langle n_1 \rangle}{d\theta} \right) = \nabla^2 n_1 - \xi^{-2} (n_1 - \langle n_1 \rangle). \quad (7)$$

Neglecting deviations of the coverage derivative from its average value makes the right-hand

member of Eq. (7) approximately zero. The resulting Helmholtz equation has a straightforward solution for $n_1(r, \theta)$ in terms of modified Bessel functions from which one can readily obtain the capture numbers σ_s .

There are cases, where the continuum approach produces an excellent agreement between the mean-field rate equations and KMC simulations, given the same assumptions about the elementary processes [18].

4.2 First-principles example of interlayer influences

In nucleation and growth of epitaxial films the morphology of the first monolayer could have great influence on the nucleation and growth of the second and subsequent layers, etc. The importance of interlayer coupling is illustrated in a very recent work on Al_2O_3 nucleation on TiC(111) [20], crucial in the deposition of $\kappa\text{-Al}_2\text{O}_3$ through chemical-vapor deposition (CVD) for the production of wear-resistant coatings on cemented-carbide cutting tools. It is found that structures characterized by the Al atoms in sites similar to the $\kappa\text{-Al}_2\text{O}_3$ structure are more favored than structures having hexagonal Al networks similar to $\alpha\text{-Al}_2\text{O}_3$. This indicated preferred growth of $\kappa\text{-Al}_2\text{O}_3$ on a perfect TiC(111) surface is understood in terms of attractive bonding between neighboring Al atoms chemisorbed on the TiC(111) surface on top of a dense O(1x1) layer (Fig. 4). This originates from the dominance of the $2p_{xy}$ orbitals of O in the O-Ti bonds in the first layer of chemisorbed O on TiC(111). Therefore, at sufficiently high Al coverage, the system finds it favorable to use the dangling O $2p_z$ bonds to bind to the next layer of chemisorbed Al atoms, provided that the antibonding Al-O orbitals that result from this find similar states in neighboring Al adatoms to form stabilizing bonds with.

4.3 First-principles account of elementary growth processes

Epitaxial growth offers an exotic variety of surface morphologies that emanate from a handful of elementary atomic diffusion processes. The first step towards a detailed understanding of

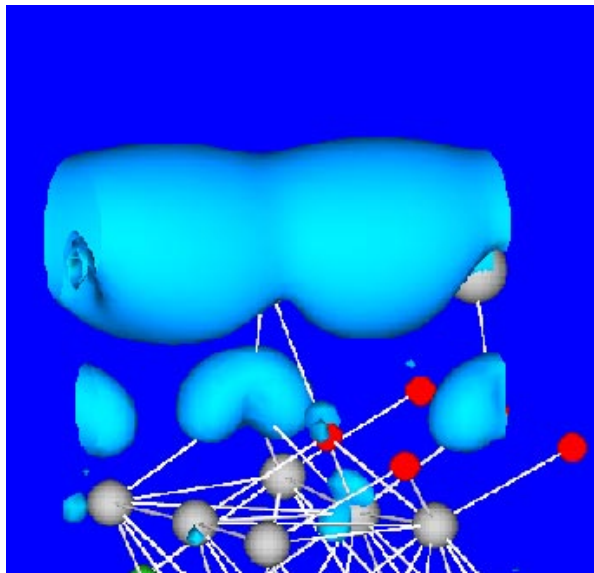


Figure 4: Local-density-of-states (LDOS) profiles describing attractive bonding between neighboring Al atoms chemisorbed on the TiC(111) surface on top of a dense O(1x1) layer [20].

this is to map out all relevant atomic processes, terrace diffusion, corner-crossing, kink-breaking and so on, which has been done on Al(111) (Fig. 5) by density-functional calculations [19]. A description with a lattice-gas model, where atoms are allowed to occupy certain grid positions only, for Al(111) the fcc and hcp sites, is adequate in epitaxy and many other situations within a broad temperature range. The diffusion of atoms adsorbed on this mesh can be described by transition-state theory (TST). Experimental techniques, such as field-ion microscopy (FIM) and STM, help to ascertain that no diffusion processes are left out.

The next step is to determine the rates for all processes. For each process i , one has to find the activation energy E_i and the corresponding prefactor ν_i^0 , yielding a collection of rates ν_i given by the Arrhenius law (TST)

$$\nu_i = \nu_i^0 e^{-E_i/k_B T}, \quad (8)$$

where k_B is the Boltzmann constant and T is the substrate temperature.

This information can be used in kinetic Monte-Carlo (KMC) simulations of growth, but the relative importance of various growth modes can be estimated (Fig. 6). From Eq. (8) an activation temperature T_i can be defined for each process i , below which the particular event is frozen out. Defining the process to be activated when it happens at a rate Γ , the onset temperature is determined by $T_i = \frac{E_i/k_B}{\ln \nu_i/\Gamma}$. The value of Γ depends on the experimental growth rate, but is typically of the order of 1/s. As the temperature is increased, more and more of these processes become activated (Fig. 6). Already around 17 K, terrace diffusion ($T_{0 \rightarrow 0}$) becomes activated. The growth occurs by a hit-and-stick mechanism, where atoms diffuse on the terraces and irreversibly attach to existing islands. By slightly raising the substrate temperature, a transition occurs from fractal to dendritic growth with ramified fractal patterns growing in three distinct directions, as observed experimentally for several different metal-on-metal systems. The asymmetry between A and B steps (Fig. 5) for several elementary diffusion processes is striking (Fig. 6).

Dimer diffusion has also been studied for Al_2 on $\text{Al}(111)$ [21] for adatom pairs on an open metal surface [23].

The next step is to make KMC simulations with energy barriers obtained from such density-functional calculations. For instance, the microscopic origin of compact triangular islands on close-packed surfaces has been identified in this way [22]: corner-diffusion anisotropy controls the shape of compact islands at intermediate temperatures. The correlation between the orientation of dendrites grown at low temperatures and triangular compact islands grown at higher temperatures (Fig. 7) is rationalized, and an explanation for why in some systems dendrites grow fat before turning compact is also provided in this way [22].

4.4 Adsorbate interactions

On surfaces there can be long-ranged forces between adsorbates, for instance, those mediated by

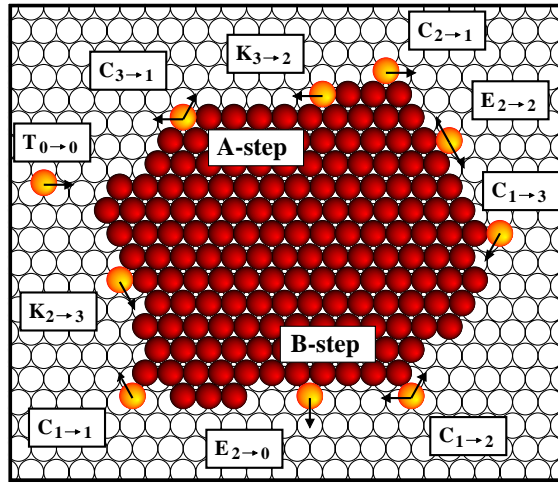


Figure 5: Elementary diffusion processes at atom islands for an fcc(111) surface [19, 22]. Each process is characterized by a letter (T for terrace, E for Edge, K for kink, and C for corner) and a subscript that indicates the number of in-layer nearest neighbors before and after the jump. The processes can take place on both A steps, with a 100 microfacet, and B steps, with a 111 microfacet.

Shockley surface states on the (111) faces of noble metals, with an oscillatory form modulated by a $1/d^2$ envelope at asymptotic adsorbate separations d . For this interaction a non-perturbative analytical estimate has been given [24], specified by experimentally accessible Shockley-state parameters and the finite Fermi-level phase shift, which characterize the standing-wave patterns observed in STM images.

This electron-mediated force is oscillatory in space, with a period related to the surface electrons' Fermi wavelength. There is alternately attraction and repulsion, as one atom "rides" the electron waves produced by the other, leading to attractive and repulsive rings surrounding each atom. This kind of indirect interactions between adatoms was suggested decades ago, but there are severe experimental problems to detect such weak long-range forces. In a new extensive and careful STM study, however, the properties of the scattered electron waves are shown to be in agreement with the non-perturbative analytical predictions [25].

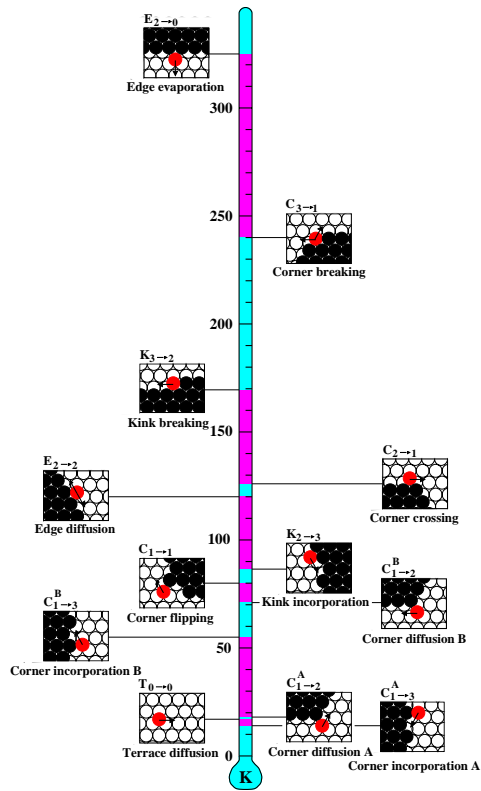


Figure 6: Temperature scale indicating the onset of elementary diffusion processes at Al islands on Al(111) [19]. The activation temperatures are calculated from Eq. (8), as described in the text. The notations are described in Fig. 5.

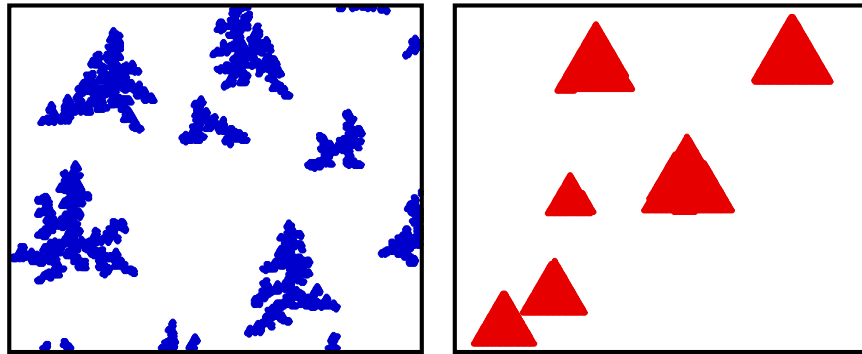


Figure 7: The island morphology calculated by KMC simulations [22] for homoepitaxial growth on Al(111) at 80 K (left) reveals dendrites with the same orientation as triangles grown at 200 K (right). In both figures the coverage is 0.10 ML and the image size $680 \times 570 \text{ \AA}^2$.

Atoms and molecules adsorbed on metals affect each other indirectly over considerable distances, not only electronically but also, *e.g.*, elastically. For intermediate distances systematic density-functional calculations have been performed [26, 28], to establish the nature and strength of such interactions, and to explain for what adsorbate systems they critically affect important materials properties. The calculations are performed with unusually large supercells (up to 336 atoms) on one of the worlds biggest computers, but the separations are still too small to make contact with the asymptotic result mentioned above. However, as shown in Fig. 8, the adatom-adatom interaction is typically oscillatory and repulsive (except for the shortest (dimer; not shown in figure) bond with adatoms in adjacent sites, where the binding energy is one order of magnitude larger (0.52, 0.26, and 0.26 eV for Al/Al(111), Cu/Cu(111), and Al/Al(100), respectively) [26].

With interaction-modified KMC simulations of epitaxial growth, a number of recent experimental reports on anomalously low diffusion prefactors are rationalized with "normal-sized" prefactors. Further, the indirect adsorbate interactions are shown to strongly alter the binding and motion of the deposited adsorbates. It is explained, where it is important to take such long-ranged interactions into account, and the KMC simulations demonstrate the strong effects they can have on surface morphology (Fig. 9). The results of the KMC simulations for low-temperature island nucleation in homoepitaxial growth on Al(111) with and without interactions between the adatoms look really different [27, 28]. With the repulsive interactions accounted for, there is a tendency towards self-organization, and the island density is significantly higher. As a function of the inverse temperature, the logarithm of the island density is shown to grow both with and without interactions (Fig. 10), however with values more than two orders of magnitude higher with interactions [26].

4.5 Mesoscale effects of interactions

Anomalous prefactors deduced from STM data have been determined by STM island-density

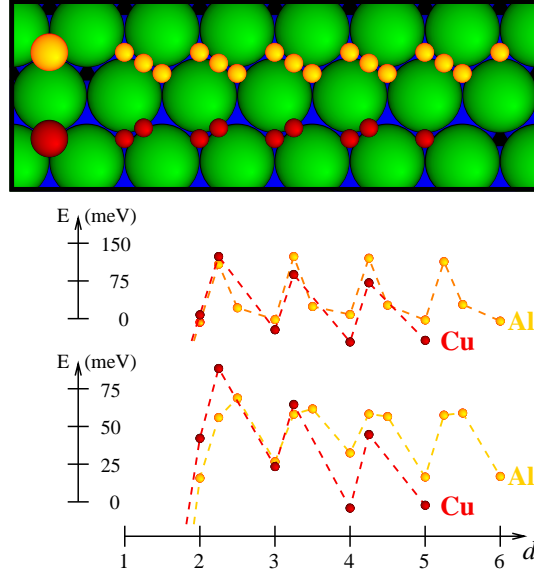


Figure 8: Top view of adsorption geometries used in the DFT calculations [26]. One adatom is placed at its preferred binding site (hcp for Al and fcc for Cu; mid-size circles), and another atom is then placed at successive binding sites and saddle points (tiny circles) along the $\langle 110 \rangle$ direction (half the length of the Al supercell is shown). The binding energy is defined as $E = E_1^1 + E_1^2 - E_0 - E_2$, where the subscript denotes the number of adatoms in the cell and the superscript identifies the individual atomic positions, and is shown as a function of adsorbate separation d in terms of lattice sites. Both frozen (middle graph) and relaxed (bottom graph) cases are truncated at short separations to enhance resolution.

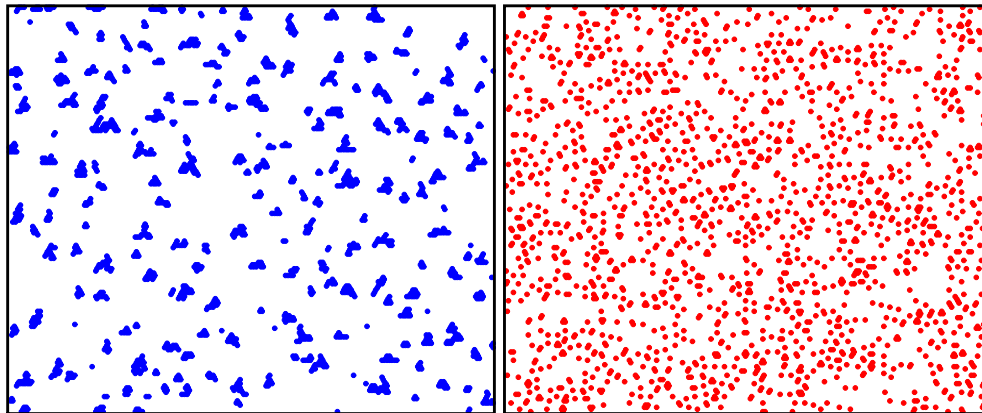


Figure 9: KMC-computed surface morphology ($500 \times 425 \text{ \AA}^2$) of Cu/Cu(111) [27, 28] at $T = 25$ K, $F = 0.01 \text{ ML/s}$, $\Theta = 5$.

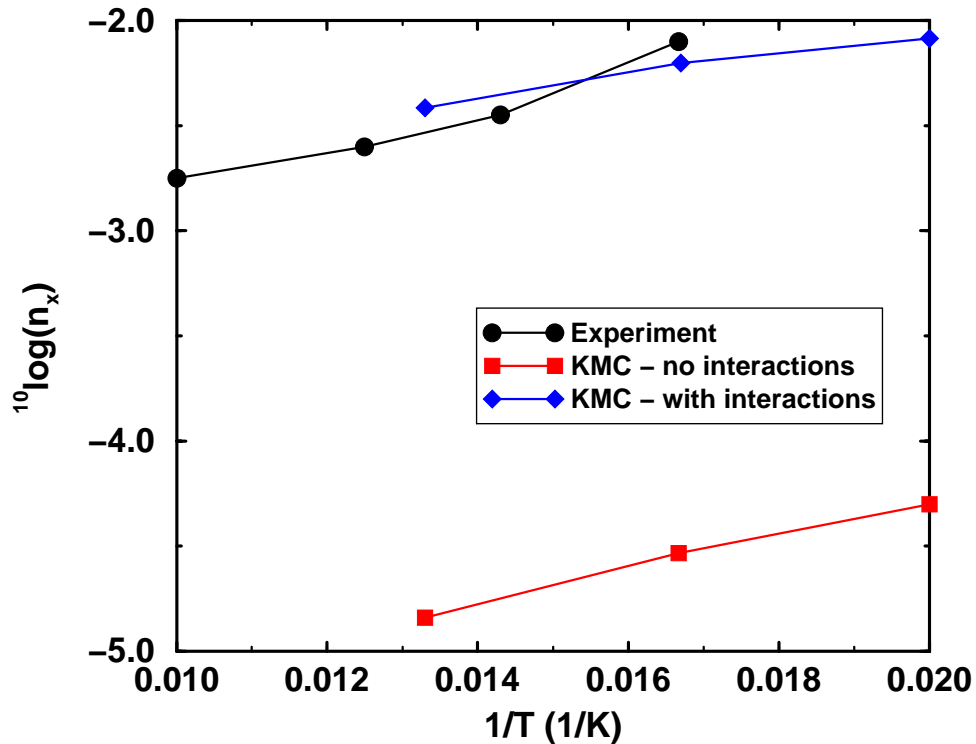


Figure 10: Island density as a function of inverse temperature from STM experiments and from KMC simulations performed with and without adatom interactions [28].

analysis using the nucleation-curve method, when Arrhenius parameters for surface diffusion are determined by gathering island-density data and then analyzing these data within mean-field nucleation theory (MFNT). According to MFNT, under certain circumstances the island density n_x relates to the monomer diffusivity D through a scaling law, $n_x \sim (\frac{F}{DN_0^2})^{1/3}$.

Adatom interactions are completely discarded in MFNT, and actually in all previous models of homogeneous nucleation. On the other hand, the above KMC simulations are performed with "normal" prefactor values and give island-density results like in experiments.

As a first attempt to account for adsorbate-adsorbate interactions in mesoscopic theory, the rate equation (7) has recently been generalized [29]. The term $\nabla^2 n_1$ in Eq. (7) is replaced by $\nabla^2(n_1 e^{\beta V_k})$, where V_k is the repulsive interaction potential and k the number of atoms in an island that interact with the adatom under consideration. The diffusion constant D is just a constant equal to $D_0 \exp(-E/kT)$, but the jump rate in different directions depends on V_k . Exactly how it is affected by V_k depends on what assumptions are made about the variation of the barrier height with V_k . Based on a rather crude approximation, namely that all barriers have the same energy (relative to some fixed energy of the system), and the fact that σ_k is rather insensitive to the actual choice, preliminary results for the dependence of the island density on the coverage $\theta = Ft$ are obtained (Fig. 11). Also in a rate-equation description, interaction effects increases the island density significantly [29].

5. Conclusions

The importance of bridging length scales for materials is stressed and illustrated by three examples, (i) nematic liquid crystals, where a field-theoretical model show strong macroscopic consequences for a simple microscopic input that can be made more versatile, (ii) strength of materials, where applicability and limitations of a mesoscopic (Peierls-Nabarro) model for dislocations are illustrated, and (iii) epitaxial growth, where microscopic findings on adsorbate

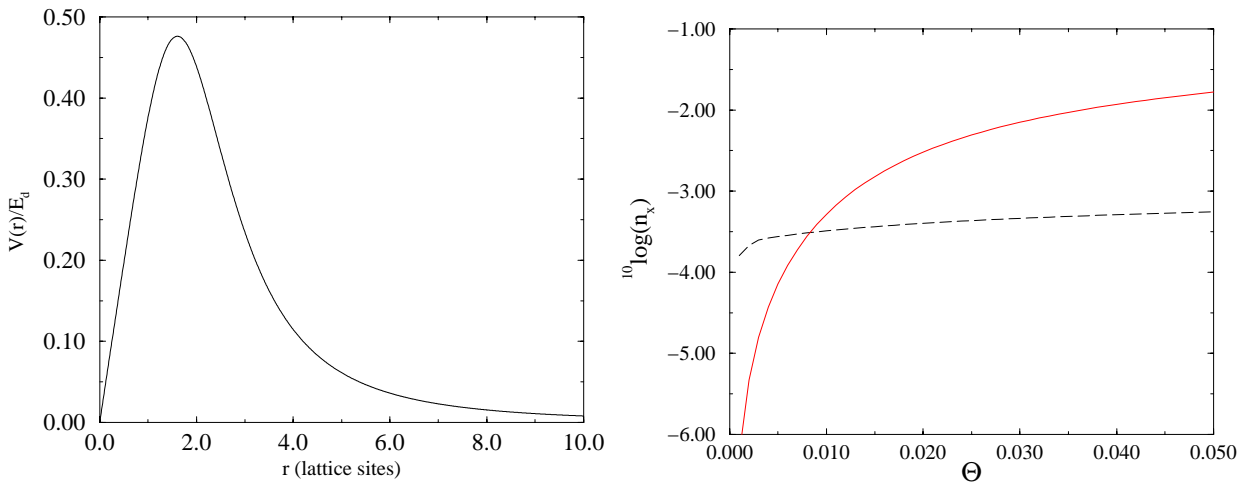


Figure 11: Island density, calculated from Eq. (7) with the interaction correction as described in Subsection 4.5, as a function of coverage. The upper graph gives the interaction potential $V(r)$ used, and the lower one the island density calculated with and without adatoms interactions.

interactions are shown to call for improvements of mesoscopic descriptions. It should be obvious from these examples that, like a famous continent, this area has a great future in a multitude of interesting and challenging things that remain to be done.

References

- [1] G.B. Olson, *Science* **277**, 1237 (1997).
- [2] E. Schröder, *Physical Review E* **62**, 8830 (2000).
- [3] R.E. Peierls, *Proc. Phys. Soc. London* **52**, 34 (1940).
- [4] F.R.N. Nabarro, *Proc. Phys. Soc. London* **59**, 256 (1947).
- [5] V. Vitek, *Phil. Mag.* **18**, 773 (1968).
- [6] J.W. Christian, V. Vitek, *Rep. Progr. Phys.* **33**, 307 (1970).

- [7] L. Hansen, K. Stokbro, B. I. Lundqvist, K.W. Jacobsen, and D. M. Deaven, Phys. Rev. Lett. **75**, 4444 (1995)
- [8] J. Hartford, B. von Sydow, G. Wahnström, and B.I. Lundqvist, Phys. Rev. B **58**, 2487 (1998).
- [9] J.P. Hirth and J. Lothe, *Theory of Dislocations*, Wiley Interscience, New York, 1982.
- [10] L.J. Teutonico, Act Met. **11**, 903 (1949).
- [11] B. von Sydow, J. Hartford, and G. Wahnström, Computational Materials Science **15**, 367 (1999).
- [12] V.V. Bulatov and E. Kaxiras, Phys. Rev. Lett. **78**, 4221 (1997).
- [13] J. Hartford , Phys. Rev. B **61**, 2221 (2000).
- [14] S.V. Dudiy, J. Hartford, and B.I. Lundqvist, Phys. Rev. Lett. **85**, 1898 (2000).
- [15] S.V. Dudiy and B.I Lundqvist, Phys. Rev. B, in press (2001).
- [16] S.V. Dudiy, Surf. Sci., in print (2001).
- [17] M. Christensen, S.V. Dudiy, G. Wahnström, to be published (2001).
- [18] G.S. Bales and D.C. Chrzan, Phys. Rev. B **50**, 6057 (1994).
- [19] A. Bogicevic, J. Strömquist, and B. I. Lundqvist, Phys. Rev. Lett. **81**, 637 (1998).
- [20] C. Ruberto, "Metastable Alumina from Theory: Bulk, Surface, and Growth of κ -Al₂O₃", PhD thesis, Chalmers University of Technology (2001), ISBN 91-7291-054-2; to be published (2001).
- [21] A. Bogicevic, P. Hyldgaard, G. Wahnström and B. I. Lundqvist, Phys. Rev. Lett. **81**, 172 (1998).

- [22] S. Ovesson, A. Bogicevic, and B. I. Lundqvist, Phys. Rev. Lett. **83**, 2608 (1999).
- [23] A. Bogicevic, S. Ovesson, B. I. Lundqvist, and D. R. Jennison, Phys. Rev. B **61**, 2456 (2000).
- [24] P. Hyldgaard and M. Persson, J. Phys.:Condens. Matter **12**, L13 (2000).
- [25] J. Repp, F. Moresco, G. Meyer, K.-H. Rieder, P. Hyldgaard, and M. Persson, Phys. Rev. Lett. **85**, 2981 (2000) — See also Physical Review Focus “Surfing the Atom’s wake,” <http://focus.aps.org/v6/st14.html> (2000); N. Knorr, H. Brune, M. Epple, A. Hirstein, M. A. Schneider, and K. Kern, submitted to Phys. Rev. Lett.
- [26] A. Bogicevic, S. Ovesson, P. Hyldgaard, B.I. Lundqvist, H. Brune, and D. R. Jennison, Phys. Rev. Lett. **85**, 1910 (2000).
- [27] S. Ovesson, Licentiate Thesis, Chalmers University of Technology (2000), Applied Physics Report 2000-30.
- [28] S. Ovesson, A. Bogicevic, G. Wahnström, and B.I. Lundqvist, Phys. Rev. B **64**, 125423 (2001).
- [29] S. Ovesson, to be published.